Aufhellung

S. L. Morelhão,ª L. H. Avanciª and S. Kyciaᵇ

ªInstituto de Física, Universidade de São Paulo, CP 66318, 05315-970 SãoPaulo, SP, Brazil, and ᵇLaboratório Nacional de Luz Síncrotron - LNLS, CP 6192, 13084-971 Campinas, SP, Brazil

Physical X-ray phase measurements are possible via three-beam diffraction experiments. Generalized and simple theoretical approaches have become a necessity for accessing this piece of information by means of practical and systematic procedures. Consistency of probabilities for the X-ray photons entering and leaving the crystal are exploited here to derive theoretical approaches accounting for *Aufhellung*, an energy balance effect among the simultaneously diffracted beams.

1. Introduction

In the *n*-beam X-ray diffraction phenomenon, or multiwave diffraction, the reduction in the intensity of a two-beam diffraction owing to the excitement of other beams is known as *Aufhellung* (Wagner, 1923; Chang, 1984). It is directly related to the balance of energy among simultaneously diffracted beams, and consequently, any theoretical description of the phenomenon must take *Aufhellung* into account to be in agreement with the most solid foundation of Physics, which is the conservation of energy.

For decades, the multiwave diffraction in single crystals has been extensively studied since it allows physical measurements of reflection phases, more precisely the invariant phase triplets (see reviews by Chang, 1984, 1998; Colella, 1995; Weckert & Hümmer, 1997). The dynamical theory – the solution for the propagation of X-rays in crystals deduced from Maxwell's equations – describes all elementary concepts of crystal optics for X-rays, and also the *n*-beam diffraction. It provides the propagation modes of the wavefields in a perfect periodic infinite medium. Boundary conditions are required for determining the amplitudes of the diffracted waves in a finite crystal, which account for the energy balance among the diffracted beams. However, great efforts have also been dedicated for developing other theoretical approaches that embrace relevant aspects of the diffraction physics, such as crystalline imperfections, and simultaneously, facilitate feasible analysis of experimental results.

The available approaches are limited solutions, mostly for *3*-beam diffraction (*3*-BD) cases, based on *2nd*-order (Juretschke, 1982; Høier & Marthinsen, 1983; Shen, 1986; Hümmer & Billy, 1986; Chang & Tang, 1988; Shen & Finkelstein, 1990; Shen & Huang, 2001; Stetsko *et al.*, 2001b) and *3rd*-order approximations derived either from Takagi-Taupin treatment (Thorkildsen *et al.*, 2001; Thorkildsen & Larsen, 2002; Okitsu, 2003) or from the fundamental equation of dynamical diffraction theory (Stetsko *et al.*, 2004); well-organized reviews on succeeding developments in this research field can be found in recent articles (Okitsu, 2003; Thorkildsen *et al.*, 2003). In most approaches, the diffracted intensities are given by

$$\mathtt{I}_G = \frac{c}{2\varepsilon_0} \left| \sum_{n=1}^{N} \mathbf{D}_{n,G} \right|^2 \qquad (1)$$

where the amplitude of the electric displacement field is written as a series expansion, and each term of the expansion, $\mathbf{D}_{n,\mathrm{G}}$, has its maximum contribution, in modulus, at the maximum of the *3*-BD excitement condition.

The motivation of this work is the fact that it is impossible to take *Aufhellung* into account by solutions in pure series expansion of the field as defined in Eq. (1); the inclusion of higher-order terms do not account for *Aufhellung* as suggested for several authors (see, for example, Stetsko *et al.*, 2004). The reason is very simple,

$$\left| \sum_{n=1}^{N} \mathbf{D}_{n,G} \right|^2 < \left| \sum_{n=1}^{N-1} \mathbf{D}_{n,G} \right|^2$$

occurs exclusively due to interference effects. It means that each additional term can reduce or enhance the diffracted intensity depending on its relative phase to the other terms of the series expansion. Individually, or in the absence of interference effects, each term represents some amount of energy contributing to the diffracted intensity, which is the opposite effect of *Aufhellung*.

The deficiency of series expansion form of solution to account for *Aufhellung* can be better demonstrated by means of an example. Let us assume a small non-absorbing crystal where third-order terms are negligible, as well as higher order ones, i.e. $\mathbf{D}_{n \geq 3,\mathrm{G}} \approx 0$. Then,

$$\begin{aligned} \mathtt{I}_0' &= \frac{c}{2\varepsilon_0} \left| \mathbf{D}_0' + \mathbf{D}_{2,0}'^{(\mathrm{A})} \right|^2 \\ \mathtt{I}_A' &= \frac{c}{2\varepsilon_0} \left| \mathbf{D}_{1,A}' \right|^2 \end{aligned} \qquad (2)$$

are the diffracted intensities under a two-beam excitement condition. When another beam is excited, for instance $\mathtt{I}_B$, the

diffracted intensities are given by

$$
\begin{aligned}
\mathtt{I}_0 &= \frac{c}{2\varepsilon_0} \left| \mathbf{D}_0 + \mathbf{D}_{2,0}^{(A)} + \mathbf{D}_{2,0}^{(B)} \right|^2 \\
\mathtt{I}_A &= \frac{c}{2\varepsilon_0} \left| \mathbf{D}_{1,A} + \mathbf{D}_{2,A}^{(B)} \right|^2 \\
\mathtt{I}_B &= \frac{c}{2\varepsilon_0} \left| \mathbf{D}_{1,B} + \mathbf{D}_{2,B}^{(A)} \right|^2 .
\end{aligned}
\tag{3}
$$

(A,B) superscripts are used on second-order waves to identify the first-order ones originating them. For instance, $\mathbf{D}_{2,0}^{(A)}$ stands for the rescattering of $\mathbf{D}_{1,A}$ towards the forward-transmitted wave, $\mathbf{D}_0$. Since the incident beam is constant in time, the total intensity of the diffracted waves under two-beam and three-beam diffraction conditions are equal, i.e.

$$
\mathtt{I}_0' + \mathtt{I}_A' = \mathtt{I}_0 + \mathtt{I}_A + \mathtt{I}_B .
\tag{4}
$$

Besides inherent difficults owing to convergence properties of the series expansions, another challenge is the time-dependent description the *3*-BD, or any multi-beam diffraction case, by series expansion solutions. It is summarized in the above example, in how to go from Eq. (2) to Eq. (3) without violating the equality in Eq. (4). In more specific words, it is necessary to described not only how the extra terms in Eq. (3) are excited, but also how the terms already excited in Eq. (2) are affected by the excitement of the new beam, $\mathtt{I}_B$ in this case. For a qualitative description, one may assume that $\mathbf{D}_0 = \mathbf{D}_0'$, $\mathbf{D}_{2,0}^{(A)} = \mathbf{D}_{2,0}'^{(A)}$, and $\mathbf{D}_{1,A} = \mathbf{D}_{1,A}'$, and that the extra terms in Eq. (3) are switched on as the crystal rotates to excite $\mathtt{I}_B$. However, in this phenomenological description the total diffracted intensity is not preserved, and that ends any possibility to correctly account for *Aufhellung*. Eventhough, such description can provide an identical result in the case of a very particular coincidence where $\mathbf{D}_{2,0}^{(B)}$ and $\mathbf{D}_{2,A}^{(B)}$ would provide destructive interferences with the other terms in $\mathtt{I}_0$ and $\mathtt{I}_A$. These destructive interference would account for the exact amount of intensity transfered to $\mathtt{I}_B$. Although some phase relationships may exist among the diffracted waves, they vary from one crystal to another since the structure factor phases are intrinsically related to the internal three-dimensional structure of the crystals. Therefore, phase relationships among the series expansion terms are not responsible for the balace of energy among the diffracted beams, i.e. for the equality in Eq. (4) of the above example.

To properly account for *Aufhellung*, we proposed here a general description of the multi-beam diffraction phenomenon based on consistency of probabilities for X-ray photons entering and leaving the crystal. Emphasis is due to the balance of energy, which appears naturally in this description. It allows convergent series expansion solutions applicable to *3*-BD cases where *Aufhellung* can not be neglected, as experimentally demonstrated here. Interference of probability amplitudes for photons – as defined for instance in the introduction of Loudon's book (Loudon, 2000) – is included to take phase sensitivity of the *3*-BD into account, and to provide mechanisms to correctly estimate the contributions of higher order terms in the solution of the diffracted wavefields. Moreover, the demon-

strative experimental dataset also carries some information on chemical bounding-charges, as shortly discussed.

2. *Three*-beam X-ray diffraction by consistency of probabilities
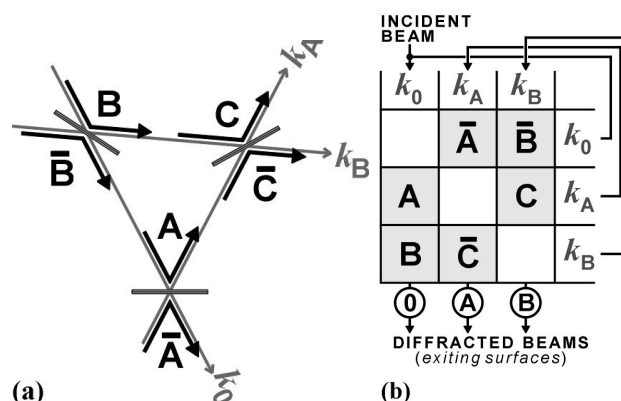
Figure 1
X-ray three-beam diffraction in crystals: (a) planar scheme of the involved A, B, C, Ā, B̄, and C̄ reflections and k_0, k_A, and k_B wavevectors; (b) diagram of probabilities where each column represents the diffraction, r_X (boxes), exiting, d_G (circles), and absorption, a_G, probabilities for X-ray photons in the beam G (G = 0, A, and B). The sum of these probabilities at each column must be equal to 1. For instance, in the incident beam column (first column at left), a forward-transmitted beam of non-diffracted photons occurs only when $d_0 = 1 - a_0 - r_A - r_B > 0$. All possible diffraction channels can be identified by following the loops of this diagrama, but in general the r_X, d_G, and a_G probabilities are dynamical variables changing at each loop.

Energy is conserved by preserving diffraction, exiting, and absorption probabilities of X-ray photons traveling in a crystal. Under *3*-BD, the photons in one diffracted beam can be further diffracted towards two other beams, as illustrated in Fig. 1(a). Each diffraction bounces the photons from one beam to another, which can be bounced again and again, or they can exit the crystal before a next bounce if not absorbed by photoelectrons or any other event that would prevent further diffraction. This is represented as a schematic diagram in Fig. 1(b). There are different diffraction channels, or zigzag route (Kato, 1976), for the photons before exiting the crystal. Channel A stands for incident photons that interact once with the lattice and leave the crystal by beam A, i.e. a single-bounce channel $k_0 \rightarrow k_A$, where reflection A is the photon-lattice interactive agent. B+C is adouble-bounce channel, $k_0 \rightarrow k_B \rightarrow k_A$, B+C+C̄ a three-bounce channel, $k_0 \rightarrow k_B \rightarrow k_A \rightarrow k_B$, and so on.

Because photons are quantum particles, interference of probability amplitudes occurs (Loudon, 2000), i.e. interference of the wavefields diffracted by different channels exiting via the same beam direction. However, in this description of the *3*-BD process, photons are initially considered as classical particles; in this context, X-ray beams "...are streams of globules, like bullets from a machine gun". The wavefields are incorporated later, for *n*-bounce channels according to the order of contribution desired in the solution of the diffracted fields.

2.1. General formalism

For general multi-beam diffraction cases, the population, $P_G(n)$, of n-bounced photons in the beam G can be calculated by introducing $p_{G,H}(n)$ as the X-ray photon diffraction probabilities from beam H to beam G after n diffraction events (bounces), then

$$P_G(n+1) = \sum_{H \neq G} p_{G,H}(n) P_H(n) . \qquad (5)$$

$P_0(0) = N_0$ stands for the incident number of photons per unit of time, and the time-dependence of these probabilities are determined by the crystal rotation, i.e. on how the crystal position varies in time until the multi-beam configuration is achieved.

Assuming a slow time variation to assure that at any time instant the populations are given by Eq. (5), their behaviors as a function of n can be infered by the sum of diffraction probabilites,

$$s_G(n) = \sum_{H \neq G} p_{H,G}(n) . \qquad (6)$$

These values are interconnected by consistency of probabilities to exiting probabilites defined as

$$d_G(n) = 1 - a_G(n) - s_G(n) \qquad (7)$$

where $a_G(n)$ is the probability of the photons in the beam G to be absorbed after n bounces. Since $d_G(n)$ is the fraction of n-bounced photons that will effectively leave the crystal via beam G, the diffracted intensities (in number of photons per unit of time) outside the crystal are given by

$$I_{G[N]} = \sum_{n=1}^{N} d_G(n) P_G(n) . \qquad (8)$$

Note that, for $N_0 = 1$ $d_G(n)P_G(n)$ corresponds to the total probability of the incident photon to interact and to leave the crystal via one of the n-bounce channels ending on beam G. It garantees the balance of energy among the diffracted beams since

$$\lim_{N \to \infty} \sum_G I_{G[N]} = N_0 , \qquad (9)$$

and hence, the converge of the series expansion in Eq. (9). However, the diffracted intensities also depend on interference effects among the probability amplitudes of the different diffraction channels. To explicitaly shown this dependence, it is necessary to replace the sum of probabilities by the modulus square of the sum of wavefields, which leads to

$$I_{G[N]} = K \left| \sum_{n=1}^{N} \sqrt{d_G(n)} \, \mathbf{D}_{n,G} \right|^2 \qquad (10)$$

where K converts wavefield square units to number of photons per unit of time diffracted within a finity solid angle. The physical meaning of $\sqrt{d_G(n)}$ is to reduce, according to Eq. (7), the probability amplitude of diffraction towards beam G when other beams are excited, i.e. when the photons on beam G, inside the crystal, have a non null probability of leaving the crystal via

other beams. Therefore, the series expansion terms of this solution do not necessarily have their maximum amplitude, in modulus, at the maximum of the multi-beam condition as found in previous approaches, e.g. Eq. (1).
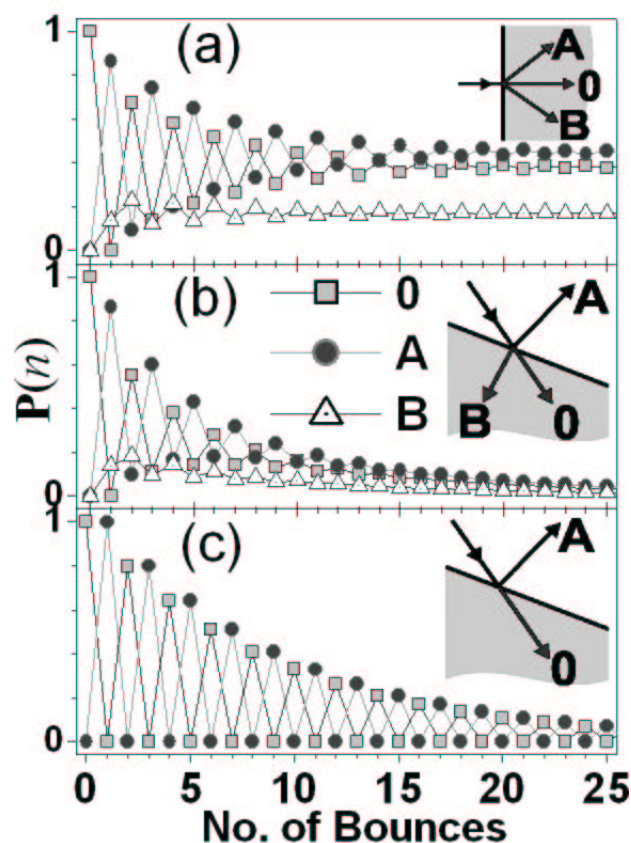
Figure 2
Populations of n-bounced photons, $P(n)$ [Eq. (11)], in the diffracted beams inside a semi-infinity crystal, calculated for $R_A = R_{\bar{A}}$, $R_B = R_{\bar{B}} = 0.16R_A$, and $R_C = R_{\bar{C}} = 0.36R_A$ where R_X is the intensity reflectivity of reflection X under 3-BD condition. (a) Laue-Laue case ($s_G = 1$): $[r_A \ r_B \ r_{\bar{A}} \ r_{\bar{C}} \ r_{\bar{B}} \ r_C] = [0.862 \ 0.138 \ 0.735 \ 0.265 \ 0.308 \ 0.692]$; (b) Bragg-Laue case ($s_A = 0.8$): $[0.862 \ 0.138 \ 0.588 \ 0.212 \ 0.308 \ 0.692]$; and (c) Bragg two-beam case ($s_A = 0.8$, $R_B = R_{\bar{C}} = 0$): $[1.0 \ 0.0 \ 0.8 \ 0.0 \ 0.0 \ 0.0]$. The r_X probabilities were obtained as $r_{A,B} = s_0 R_{A,B}/(R_A + R_B)$, $r_{\bar{A},\bar{C}} = s_A R_{\bar{A},\bar{C}}/(R_{\bar{A}} + R_{\bar{C}})$, and $r_{\bar{B},C} = s_B R_{\bar{B},C}/(R_{\bar{B}} + R_C)$.

Limited to 3-beam diffraction cases, the $p_{G,H}$ diffraction probabilities are rewritten for sake of simplicity as r_X where $X (= A, B, C, \bar{A}, \bar{B}, \text{ or } \bar{C})$ indicates the Bragg reflection transfering energy from beam H to beam G, as shown in Fig. 1(b). Henceforth, Eq. (5) become

$$\begin{aligned}
P_0(n+1) &= r_{\bar{A}} P_A(n) + r_{\bar{B}} P_B(n) \\
P_A(n+1) &= r_A P_0(n) + r_C P_B(n) \qquad (11) \\
P_B(n+1) &= r_B P_0(n) + r_{\bar{C}} P_A(n) .
\end{aligned}$$

research papers

2.2. Diffraction geometries and exiting probabilities

To achieve some insights on the intrinsic correlation among diffraction geometries and exiting probabilities, a few cases are discussed in this subsection.

In Laue-Laue diffraction geometry there are three diffracted-'transmitted' beams, as illustrated in the inset of Fig. 2(a). A non-absorbing semi-infinity crystal in this geometry is represented by $s_G = 1$, and hence $a_G = d_G = 0$. Since $r_A + r_B = 1$, $r_{\bar{A}} + r_{\bar{C}} = 1$, and $r_{\bar{B}} + r_C = 1$ the photons are bouncing endlessly from one beam to another, and the photon populations tend to constant non-null values, as shown in Fig. 2(a). No diffracted beams are measured outside the crystal, $I_G = 0$, since the photons will never reach the exiting surface at infinity. On the other hand, for a finite crystal slab there would be a minimum number of bounces, n_L, necessary for the photons to reach the exiting surface. Then, for $n < n_L$ the exiting probabilities are zero, $d_G \approx 0$, and the behavior of the populations are very similar to that shown in Fig. 2(a); but, for $n > n_L$ the populations vanish and diffracted beams are measurables as $I_G \approx \{P_G(n_L)$ since $d_G(n_L) \approx 1$ in Eq. (8).

A different situation occurs when absorption or exiting probabilities are not null, and hence $s_G < 1$. In this case, all populations decrease as a function of n, as for instance depicted in Fig. 2(b) where the only difference with respect to Fig. 2(a) is that $s_A = 0.8$, or $d_A + a_A = 0.2$. If $d_A = 0$ the decrease of the populations is owing to absorption only, and the diffracted intensities are still zero. However, for $0 < d_A < 0.2$ some photons on beam A can reach an exiting surface and then $I_A > 0$. In a semi-infinite crystal it means that the beam A must be a Bragg-reflected beam; a Bragg-Laue diffraction geometry as illustrated in the inset of Fig. 2(b). A Bragg-Bragg diffraction geometry would require $d_A > 0$ and $d_B > 0$.

Away from the *3*-BD condition, when only reflection A is excited, there is a total transference of energy (number of photons) from one beam to the other, as observed in Fig. 2(c). In this particular example, all photons in the beam 0 are bounced towards beam A, and 80

It is very convenient to take exiting and diffraction probabilities as constant values instead of functions of n. These values are dynamical variables changing at each bounce owing either to the relative positioning of the exiting surfaces and polarization factors. In principle, it is possible to calculate the diffraction probabilities per unit of length and to compute the polarization factors for each sequence of reflections. However, before upgrading the proposed approach to more realistic cases and to include interference effects according to Eq. (10), it is necessary to demonstrated that Eq. (8) is a time-dependent solution capable to describe the excitament of beams without violating the equality in Eq. (9), and hence capable to account for *Aufhellung*.

2.3. Time-dependent solutions

The basic requirement for a time-dependent solution is to preserve the sum of probabilities in Eq. (7) as one or more diffraction probabilities change in time owing to the crystal's rotation. The first effect to be analysed is the sharing of energy between

two reflections simultaneously diffracting a given beam, as for instance the A and B, $\bar{A}$ and $\bar{C}$, or $\bar{B}$ and C reflections in Fig. 1(a).
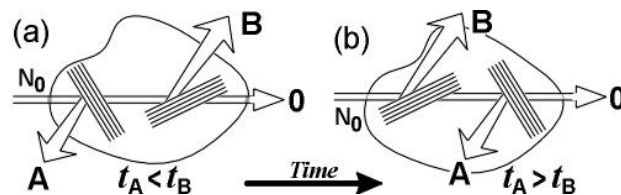
Figure 3
Simultaneousness of diffraction events and their effects on the diffracted intensities. (a) Reflection A occurs before reflection B: $I_A = R_A N_0$, $I_B = R_B(1 - R_A)N_0$, and $I_0 = (1 - R_B)(1 - R_A)N_0$. (b) Reflection B occurs before reflection A: $I_B = R_B N_0$, $I_A = R_A(1 - R_B)N_0$, and $I_0 = (1 - R_A)(1 - R_B)N_0$. For time coincidental reflections, the outcome is the average of (a) and (b): $I_A = R_A(1 - 0.5R_B)N_0$ and $I_B = R_B(1 - 0.5R_A)N_0$.

For this demonstration, assume a very small non-absorbing crystal where R_X is the kinematical intensity reflectivity of reflection X, so that $I_X = R_X N_0$ and $I_0 = (1 - R_X)N_0$. Note that, according to this definition of reflectivity $0 \leq R_X \leq 1$. When only reflection A is excited the non-null populations of photons are $P_0(0) = N_0$ and $P_A(1) = R_A N_0$, and then, the kinematical intensities according to Eq. (8) are obtained for $d_0 = 1 - R_A$, $r_A = R_A$, and $d_A = 1$, which satisfy $d_0 + r_A = 1$.

The problem in describing the excitement of reflection B, when A is already excited, is that $d_0 + r_A + r_B > 1$ if we take $r_A = R_A$ and $r_B = R_B$. It implies that the previous exiting and diffraction probabilities, d_0 and r_A, must decrease when reflection B is excited. It seems to be a complicated problem because reflections A and B are simultaneous events in time; otherwise would be very simple to calculate the diffracted intensities as demonstrated in Fig. 3. In fact, the correct values of diffraction probabilities are obtained from the average diffracted intensities between the two hypothetical situations shown in Figs. 3(a) and 3(b).

$$r_A = R_A(1 - 0.5R_B), \quad r_B = R_B(1 - 0.5R_A), \qquad (12a)$$

and

$$s_0 = R_A + R_B - R_A R_B . \qquad (12b)$$

Note that these equations have a perfect simmetry with respect to the excitament of one reflection, B or A, when the other, A or B, is already excited. It is an important condition that must be present in any theoretical description of simultaneous diffraction processes. Eqs. (12) also provide how much the previous diffraction probability varies owing to the other reflection, as well as the exiting probability since $d_0 = 1 - s_0$. This solution always satisfy the consistency of probability, Eq. (7), if the maximum value of s_0, s_0^{max}, is given in the range from 0 to 1-a_0 ($a_0 = 0$ in non-absorbing crystals). This maximum value occurs when both reflections are at their respective maxima.

To effectively calculate the sharing of energy between two reflections, values either for s_0^{max} and α_{BA} (the kinematical reflectivity ratio) must be provided. Then,

$$R_B = \alpha_{BA} R_A \qquad (13a)$$

and from Eq. (12b)

$$R_A = \kappa - \sqrt{\kappa^2 - s_0^{max}/\alpha_{BA}} \qquad (13b)$$

where $\kappa = 0.5(1 + \alpha_{BA})/\alpha_{BA}$, and $R_{A,B} = s_0^{max}$ if $R_{B,A} = 0$.

Every bounces of photons inside large crystals are localized kinematical diffraction processes, as for instance assumed by Darwin (1914) or Zachariasen (1945) when describing primary and secondary extinction phenomena. According to this assumption, Eqs. (12) and Eqs. (13) are also valid for calculating the diffraction probabilities after n bounces, to which values for $s_0^{max}(n)$ are required. Moreover, the diffraction probabilities for the other two couples of reflections, in Fig. 1(b), are also calculated by analogous equations, i.e. $r_{\bar{A}(\bar{B})}$ and $r_{\bar{C}(C)}$ are obtained by replacing A and B by $\bar{A}(\bar{B})$ and $\bar{C}(C)$ in Eqs. (13) and Eqs. (12).

Knowledge on the $s_G^{max}(n)$ values as well as on the kinematical reflectivity ratios allow an almost-full description, besides interference effects, of the *3*-BD process as a function of the crystal's rotation. The great success of this approach is that at any instant of time the condition imposed by Eq. (9) is always satisfied, as demonstrated below.

2.4. *Aufhellung*

Occurance of *Aufhellung* as a direct consequence of energy balance mechanisms is investigated here for a few hypothetical cases, shown in Fig. (4), where the $s_G^{max}(n)$ are taken by constant values as a function of n. It can be a very good approximattion when the populations of photons become neglectable just after a few bounces.

Azimuthal rotation of the crystal around the diffraction vector of reflection A is a possible systematic procedure to also bring reflection B to a diffraction condition, and hence to achieve the *3*-BD configuration in Fig. 1(a). To describe the effects of the ϕ rotation on the diffracted intensities, $R_{B,\bar{C}}$ in Eqs. (12) are now multipled by $L(\Delta\phi)$, a lorentzian function of unit weight, $L(\Delta\phi = 0) = 1$. $\Delta\phi = \phi - \phi_0$ stands for the deviation in the rotation angle, ϕ, from the *3*-BD condition at ϕ_0.

For a give value of $\Delta\phi$, the intensities are calculated by Eq. (8), $P_G(n)$ by Eq. (11), r_X by Eqs. (12a), and $d_G(n) = 1 - a_G - s_G$ by Eq. (12b). The R_X values are obtained by Eqs. (13); these reflectivity values do not depend on $L(\Delta\phi)$. The exact calculation routine of the intensities profiles in Fig. 4 are given in Appendix A, where six input values are required: the structure factor modulii, $|F_A| = |F_{\bar{A}}|$, $|F_B| = |F_{\bar{B}}|$, and $|F_A| = |F_{\bar{A}}|$, as well as the s_G^{max} values. It has been implicitaly assume, for this demonstration only, that the kinematical intensity-reflectivity ratios are given by the modulus square of the structure factors, e.g. $\alpha_{BA} = |F_B|^2/|F_A|^2$ in Eq. (13b).

As the crystal rotates, we go from a two-beam case, I_0 and I_A, to a three-beam case where I_B is also excited. But, at any instant,

$$I_0 + I_A + I_B = N_0$$

since $a_G = 0$, as can be observed in all cases shown in Fig. 4. This is the relevant point that we have wished to demonstrate.

Some interesting situations are investigated in Fig. 4. Since I_B varies from 0 to a maximum value at $\Delta\phi = 0$, *Aufhellung* occurs on the two-beam intensities only. Reduction in the diffracted-'transmited' beam, I_0, is observed in all cases, although not visible in Fig. 4(d), mainly because of the chosen high value for $s_0^{max} = 0.8$; it favors the transference of energy to the other beams. In Fig. 4(a) *Aufhellung* is also observed in I_A, and the major reason is the fact that the exiting probabilities via beam B are higher than via beam A; $d_A < d_B$ although $|F_A| < |F_B|$. By just exchanging the ration between these exiting probabilities, I_A shows an *Umweganregung* peak (Renninger, 1937), Fig. 4(b), instead of the *Aufhellung* dip in Fig. 4(a). When reflection B is forbidden, $|F_B| = 0$, the intensity of beam B is due to higher order channels, e.g. A+$\bar{C}$, but *Aufhellung* is still observed, Fig. 4(c). It is also a dominant effect on I_A when reflection C is forbidden, $|F_C| = 0$, in Fig. 4(d).
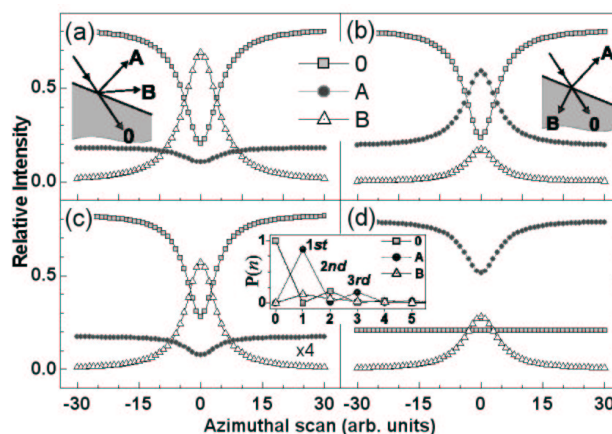
Figure 4
Energy balance effects on three-beam diffraction intensities as a function of azimuthal scans around the diffraction vector of reflection A, which is kept excited during the scans. (a) Bragg-Bragg case calculated with the parameter vector p = [$|F_A|$ $|F_B|$ $|F_C|$ s_0^{max} s_A^{max} s_B^{max}]=[2 4 6 0.8 0.4 0.2]; (b) Bragg-Laue case: p = [2 4 6 0.8 0.4 0.8]; (c) p = [2 4 0 0.8 0.1 0.4]; and (d) p = [2 0 6 0.8 0.4 0.1]. The intensities are calculated by Eq. (8), see Appendix A for more details. The p values provide here have been chosen for illustrative purposes only.

2.5. Amplitude and interference of the diffracted wavefields

There is an infinity number of possibilities for the r_H values depending on diffraction geometry, absorption, and reflectivity of the involved reflections. All *3*-BD cases are describable by some set of r_H values under the scope of Eq. (**??**), which was useful to demonstrate the physical meaning of the *Aufhellung* term. However, to accomplish a complete description of the *3*-BD phenomenon, it is necessary to account for interference effects, or quantum entanglement, among the probability amplitudes of the different routes inside the crystal. Therefore, we must work with the wavefields and not only with the number of photons scattered by each diffraction channel. For a Bragg reflected primary beam, a complete description is accomplished by assigning wavefields to every *Umweg* channel and replacing

the sum of their probabilities by the modulus square of the sum of their wavefields, i.e.,

$$\sum_{n=1}^{N} P_A(n) \rightarrow \left| \sum_{n=1}^{N} \mathbf{D}_A(n) \right|^2 = |\mathbf{D}_N(\phi)|^2$$

where $\mathbf{D}_A(n)$ is the total wavefield diffracted by all n-bounce channels ending on the beam A, for instance,

$$\begin{aligned} \mathbf{D}_A(1) &= \boldsymbol{D}_A, \\ \mathbf{D}_A(2) &= \boldsymbol{D}_{BC}(\phi), \\ \mathbf{D}_A(3) &= \boldsymbol{D}_{A\bar{A}A} + \boldsymbol{D}_{B\bar{B}A}(\phi) + \boldsymbol{D}_{A\bar{C}C}(\phi), \dots. \end{aligned}$$

The oscillation directions of the wavefields are determined by polarization factors, while their amplitudes are related to the diffraction probabilities according to

$$K|\boldsymbol{D}_A|^2 = \mathrm{I}_0 \mathrm{r}_A \boldsymbol{\nu}_A^2, \quad K|\boldsymbol{D}_{BC}(\phi)|^2 = \mathrm{I}_0 \mathrm{r}_B \mathrm{r}_C \boldsymbol{\nu}_{BC}^2, \dots$$

where K converts wavefield square units to number of photons per unit of time, and the dependence with the azimuthal angle, ϕ, is owing to r_B and $\mathrm{r}_{\bar{C}}$ probabilities, see Eq. (11). The polarization factor of each individual channel, $\boldsymbol{\nu}_A$, $\boldsymbol{\nu}_{BC}$, ..., are calculated as described in the Appendix A. With these definitions, the intensity equation, Eq. (**??**), can be written in terms of the Nth-order solution of the primary wavefield, $\mathbf{D}_N(\phi)$, as

$$\mathrm{I}_{A[N]}(\phi) = K[1 - (\mathrm{a}_A + \mathrm{r}_{\bar{A}} + \mathrm{r}_{\bar{C}})]|\mathbf{D}_N(\phi)|^2. \qquad (14)$$

There are two basic differences between the intensity equation obtained here by consistency of probabilities, Eq. (14), and those obtained by a pure series expansion as in Eq. (1). The first, and most obvious difference, is the *Aufhellung* term multiplying the modulus square of the series expansion of the field, $|\mathbf{D}_N(\phi)|^2$; and the second difference is the fact that the amplitude of each term of the series expansion, i.e. of each diffraction channel, does also depend explicitly of the diffraction probabilities. Therefore, Eq. (14) is an outstanding tool for qualitative understanding of the *3*-BD process because, once the diffraction, absorption and exiting probabilities are estimated, the balance of energy and the relative relevance of the terms in the series expansion are determined. To keep our focus in demonstrating the necessity of the *Aufhellung* term for describing the *3*-BD process, a detailed suggestion on how to estimated the diffraction probabilities and the amplitudes of the fields for a linearly polarized X-ray beam is left to Appendix A.

Since the dependence of the wavefields with the azimuthal scan can be taken into account by a simple function, $\mathtt{f}(\phi)$, where $|\mathtt{f}(\phi)|^2 = 1$ at the maximum of the *3*-BD, the 3rd-order solution of the primary wavefield, $\mathbf{D}_3(\phi)$, can be written as a 5×3 matrix (5 vectors, 3 components each):

$$[\mathrm{D}_{\alpha j}] = \begin{bmatrix} \boldsymbol{D}_A \\ \boldsymbol{D}_{BC}\mathtt{f}(\phi)e^{i\Psi_T} \\ \boldsymbol{D}_{A\bar{A}A}e^{i\Delta\delta_A} \\ \boldsymbol{D}_{B\bar{B}A}\mathtt{f}(\phi)e^{i\Delta\delta_B} \\ \boldsymbol{D}_{A\bar{C}C}\mathtt{f}(\phi)e^{i\Delta\delta_C} \end{bmatrix} \qquad (15)$$

where $\Psi_T = \delta_B + \delta_C - \delta_A$ is the invariant phase triplet, $\Delta\delta_G = \delta_G + \delta_{\bar{G}}$, and δ_G is the phase of the structure factor of reflection G. The choice of a same $\mathtt{f}(\phi)$ function to all ϕ-dependent channels (or terms of the series expansion) as well as $\mathtt{f}(\phi)$ itself can be subject of further discussion, but it is out of scope here since there are other equivalent formats of Eq. (15) already available in the literature, see for example Eqs. (20), (21), and (22) of Thorkildsen & Larsen (2002) or Eq. (7) of Stetsko *et al.* (2004). $\mathtt{f}(\phi)$ stands for the resonant term taking into account the dynamical phase shift of the multiple excited waves (see also Shen *et al.*, 2001; Weckert & Hümmer, 1997). Then, the intensity of the primary beam is given by

$$\mathrm{I}_{A[3]}(\phi) = K'[1 - b|\mathtt{f}(\phi)|^2] \sum_{\alpha,\beta=1}^{5} \xi_{\alpha\beta} \sum_{j=1}^{3} \mathrm{D}_{\alpha j}\mathrm{D}_{\beta j}^*. \qquad (16)$$

$\mathrm{r}_{\bar{C}}(\phi)$ has been replaced by $\mathrm{r}_{\bar{C}}|\mathtt{f}(\phi)|^2$ in the *Aufhellung* term. $K' = K(1 - \mathrm{a}_A - \mathrm{r}_{\bar{A}})$ and $b = \mathrm{r}_{\bar{C}}/(1 - \mathrm{a}_A - \mathrm{r}_{\bar{A}})$ stands for the fraction of the primary intensity taken by the secondary beam. The $\xi_{\alpha\beta}$ coefficients can be used to artificially tune the coherence, or interference capability, of the wavefields in Eq. (15). For a maximum coherence, $\xi_{\alpha\beta} = 1$; otherwise $\xi_{\alpha\alpha} = 1$ and $0 \leq \xi_{\alpha\beta} = \xi_{\beta\alpha} < 1$.
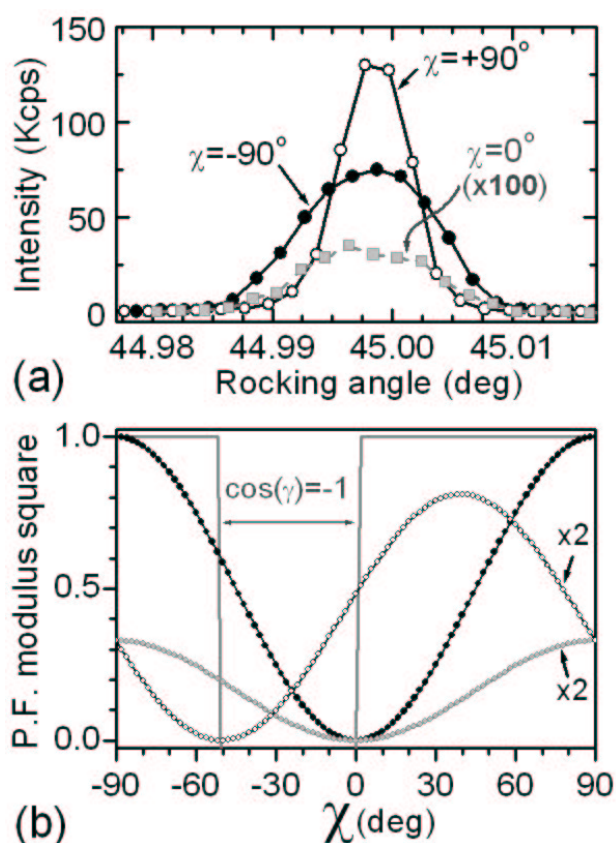
Figure 5
(a) Rocking curves of the $2\bar{2}6$ GaSb primary reflection with the incidence plane at the horizontal position, π-polarization ($\chi = 0$), and at the vertical, σ-polarization, scattering upwards ($\chi = +90°$) and downwards ($\chi = -90°$). (b) Modulus square of the polarization factors (P.F.): v_A and $v_{A\bar{A}A}$ (closed-black circles), v_{BC} and $v_{B\bar{B}C}$ (open circles), and $v_{A\bar{C}C}$ (gray circles) calculated as described in Appendix A. The latter two curves are multiplied by two in the given scale. $\cos\gamma$ (gray line) is equal to -1 in the interval $-50.8° < \chi < 0$ ($D_A \wedge D_{BC} = \gamma$). These five polarization factor are either parallel or anti-parallel to each other; it is a consequence of $2\theta_A = 90°$ (Bragg angle of the primary reflection equal to 45°). For other values of $2\theta_A$, the polarization factors have, in general, different directions.

3. Experimental and simulated results

The most simple experiment to prove that *Aufhellung*, as considered in Eq. (16), is necessary for describing the *3*-BD process would be by eliminating from $\mathbf{D}_3(\phi)$, Eq. (15), the contributions of all ϕ-dependent *Umweg* channels. Then, a symmetric dip owing to *Aufhellung* should be observed in the ϕ-scan. In fact, the linear polarization of the synchrotron radiation can be used to eliminate simultaneously the contributions from the B+C and B+$\bar{B}$+A channels. By setting the secondary reflection forbidden by polarization ($v_B \approx 0 \Rightarrow D_{BC} \approx D_{B\bar{B}A} \approx 0$), the only ϕ-dependent features in $\mathtt{I}_{A[3]}(\phi)$ are provided by *Aufhellung*, $b \neq 0$, besides the contribution from the A+$\bar{A}$+C channel ($D_{A\bar{C}C} \neq 0$).

This experiment was carried out at the Brazilian Synchrotron Light Laboratory (LNLS), X-ray diffraction beamline (XRD1), with the polarimeter-like diffractometer described elsewhere

(Morelhão, 2003). The rotation of the diffractometer's incidence plane around the incident beam direction is provided by the χ-axis. With $\chi = 0$ the incidence plane is at the horizontal position (π-polarization), and it is at the vertical position (σ-polarization) scattering upwards or downwards for $\chi = +90°$ or $\chi = -90°$, respectively. The X-ray photon energy has been set to 9539eV by a Si 111 double-crystal monochromator, the horizontal beam divergence is limited by slits, and the sample is a GaSb (001) crystal. The rocking curves of the $\bar{2}26$ GaSb primary reflection at $\chi = -90°$, 0, and $+90°$ positions of the incidence plane are shown in Fig. 4(a), while the behavior of the polarization factors for the chosen *3*-BD as a function of χ are shown in Fig. 4(b).

The experimental interference profiles (ϕ-scans) of the $\bar{2}26/\bar{2}\bar{2}6/040$ three-beam diffraction (A/B/C reflections) are shown in Fig. 5 as a function of the polarization direction of the incident X-ray beam. The ϕ-scans where *Aufhellung* is dominant are marked by a dashed circle. Best-fitting curves are also shown. They were adjusted to the experimental data using the *2nd*-order approximation, $\mathtt{I}_{A[2]}(\phi)$, derived from Eq. (16) by setting $\xi_{\alpha\beta} = 0$ for α, $\beta \geq 3$, and $\xi_{12} = \xi_{21} = \xi$. $\mathtt{f}(\phi) = w/[2(\phi - \phi_0) - iw]$, w is the intrinsic width, $i = \sqrt{-1}$, and $\phi_0 = 150.5645°$ since the [110] was taken as the reference direction for the ϕ-rotation. The instrumental broadening is taken into account by a gaussian convolution (FWHM=w_G) where the range of the numerical integral is $5w_G$. With $\Psi_T = 0$ (the theoretical values in the absence of anomalous scattering), the other adjustable parameters have been optimized by a fitting algorithm within the following ranges of allowed values: $R = \sqrt{r_B r_C/r_A}$, [0.5 : 1.5]; ξ, [0.4 : 0.8]; b, [0 : 1]; and w, [0.0012° : 0.0024°]. There are several combination of these parameters capable to reproduce the same best-fitting curves, but in general, the instrumental width, w_G, varies from about 0.003° to 0.008° as the incidence plane goes from the horizontal to the vertical position.

The observed changes in the asymmetry of the profiles can be understood by analyzing the behavior of the polarization factors, Fig. 4(b). Since the Bragg angle of the primary and secondary reflections are 45° ($\lambda = 1.2998$Å), the signal of

$$\cos\gamma = \mathbf{D}_A \cdot \mathbf{D}_{BD}/|\mathbf{D}_A||\mathbf{D}_{BD}|$$

abruptly change twice, at $\chi = 0$ ($v_A \approx 0$) and $\chi = -50.8°$ ($v_B \approx 0$) where the A and B reflections are forbidden, respectively. For $\chi > 0.0°$ or $\chi < -50.8°$, the five fields contributing to $\mathbf{D}_3(\phi)$, Eq. (15), are parallel, i.e. they have σ-components only. In the χ range where $\cos\gamma = -1$, $\mathbf{D}_{BC}$ and $\mathbf{D}_{B\bar{B}A}$ are anti-parallel to the other fields, and therefore, the asymmetry of the profiles are reversed.

To clearly demonstrate the *Aufhellung* effect, we have searched for a set of diffraction probabilities capable to reproduce, at least qualitatively, all scans in the experimental dataset, and not only the scan where this effect is dominant. Therefore, for qualitative comparison purposes only, the set of ϕ-scans generated by the *3rd*-order solution of the intensity equation, Eq. (16), is shown in Fig. 6. They were calculated for the same polarizations of those scans in Fig. 5. The diffraction probabilities, $[r_A\ r_B\ r_{\bar{A}}\ r_{\bar{C}}\ r_{\bar{B}}\ r_C] = [0.31\ 0.49\ 0.025\ 0.455\ 0.092\ 0.758]$,

as well as the intrinsic width, $w = 0.0016°$, coherence coefficients, $\xi_{\alpha\beta} = 0.6$ (for $\alpha \neq \beta$), and the invariant phase triplet, $\Psi_T = 30.0°$, were obtained by trial and error, based on visual comparison with the dataset in Fig. 5. $\Delta\delta_A = \Delta\delta_B = \Delta\delta_C = 0.0°$ (theoretical values without anomalous scattering). The instrumental width is the unique parameter, besides the polarization angle, that changes from one ϕ-scan to the other, according to the values extracted in the fitting procedure of the experimental dataset above mentioned. Different values of the incident intensity were used to generate the scans with $\chi < 0°$ ($I_0 = 228$ Kcps) and with $\chi > 0°$ ($I_0 = 441$ Kcps). It was necessary to match the peak intensity of the primary reflection, which is different when scattering downwards and upwards as shown in Fig. 4(a). Moreover, to achieve such agreement to all ϕ-scans in the experimental dataset (Fig. 5), the excitation function of the A+C̄+C channel was replaced by $-f^*(\phi)$.

Fig. 7 shows the experimental and simulated ϕ-scans where $D_{BC} \approx D_{B\bar{B}A} \approx 0$ ($\chi = -52°$) as well as where their values, in modulus, are close to a maximum ($\chi = 56°$). Besides the scans already shown in Figs. 4 and 5, there are two other simulated scans, both generated by Eq. (16) with exactly the same parameters described in the above paragraph, but without accounting for *Aufhellung*, i.e. $b = 0$, and for $\Delta\delta_C = 80.0°$. The primary intensities, base lines of the scans, were matched by displacing the intensity scale of the experimental scans.

4. Discussions

Only on theoretical basis, it is possible to assure that an *Aufhellung* term, such as $[1 - b|f(\phi)|^2]$ in Eq. (16), is required for a complete description of the *3*-BD phenomenon by any theoretical approach where the solution of the total diffracted wavefield is written as series expansion. Otherwise, the *Aufhellung* effect would depend on the relative phases of the terms in the series expansion. The result in Fig. 7(a) proves it experimentally. Since D_{BC} and $D_{B\bar{B}A}$ were eliminated by the linear polarization of the synchrotron radiation, the only possible way to generate a dip-like feature in this ϕ-scan is by assigning to $\Delta\delta_C$ a phase value close to 90°, as shown by the dashed curve in Fig. 7(a). Actually, this phase value is close to zero. If anomalous dispersion is taken into account for X-ray photons of 9539eV, $\Delta\delta_C \simeq 11°$ ($f'_{Ga} = -2.172$, $f''_{Ga} = 0.572$, $f'_{Sb} = 0.105$, and $f''_{Sb} = 4.434$). However, even if it was close to 90°, interpretation of *Aufhellung* as a phase dependent feature is conceptually wrong. For instance, without the *Aufhellung* term, $b = 0$, the interference of D_A and $D_{A\bar{C}C}$ would produce an asymmetric profile, such as the gray one in Fig. 7(a), which does not account for the pull of energy owing to the excitement of the secondary beam. – One might be wondering, what secondary beam are the authors talking about? Is the secondary reflection forbidden by polarization or not? – Although, the $\bar{2}\bar{2}6$ reflection is forbidden, or suppressed, at this polarization, the secondary beam intensity is owing to photons exiting the crystal by the A+C̄ *Aufhellung* channel, which has a higher exiting probability than the A+C̄+C *Umweg* channel. Moreover, the ϕ-scans in Fig. 7(b) have shown that even when the B+C *Umweg* channel provides a strong contribution, the *Aufhellung* effect can significantly change the asymmetry of the interference profiles.
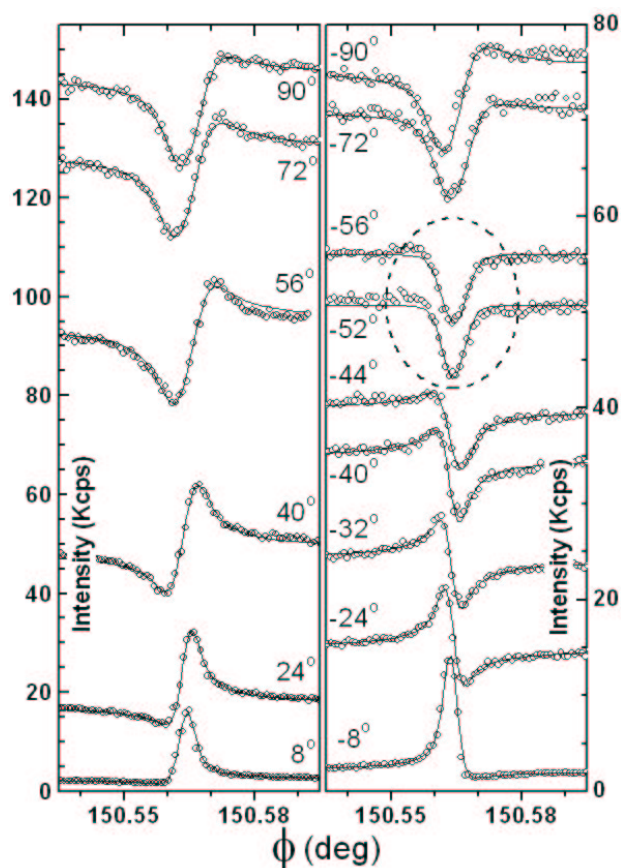
Figure 6
Experimental (open circles) three-beam X-ray diffraction interference profiles, ϕ-scans, as a function of the polarization angle χ, given aside of each scan. The A (primary), B (secondary), and C (coupling) reflections are the $\bar{2}26$, $\bar{2}\bar{2}6$, and 040 reflections of a GaSb (001) crystal, respectively. X-ray photon energy is 9539eV. The best-fitting curves (solid lines) were obtained by 2*nd*-order solution of the intensity equation, $I_{A[2]}(\phi)$, after a gaussian convolution to account for the instrumental broadening, as explained in the text (§3). The profiles where *Aufhellung* is a dominant effect are marked by a dashed circle. They correspond to polarizations around $\chi = -50.8°$ where $D_{BC} \simeq D_{B\bar{B}A} \simeq 0$, see Fig. 4(b).

Note that the statements in the above paragraph are valid independently on how the terms of the series expansion – the wavefields in Eq. (15) for a 3*rd*-order solution – are calculated or described as a function of the azimuthal and incidence angles. As far as their maximum values, in modulus, occur at the maximum of the *3*-BD excitement condition, the statements stand. Replacing $f(\phi)$ by any other function changes only how the asymmetry of the interference profiles are affected by the phase values; and by using non-unit coherence coefficients ($\xi_{\alpha\beta} < 1$ for $\alpha \neq \beta$), we are just smoothing the asymmetries of the profiles.
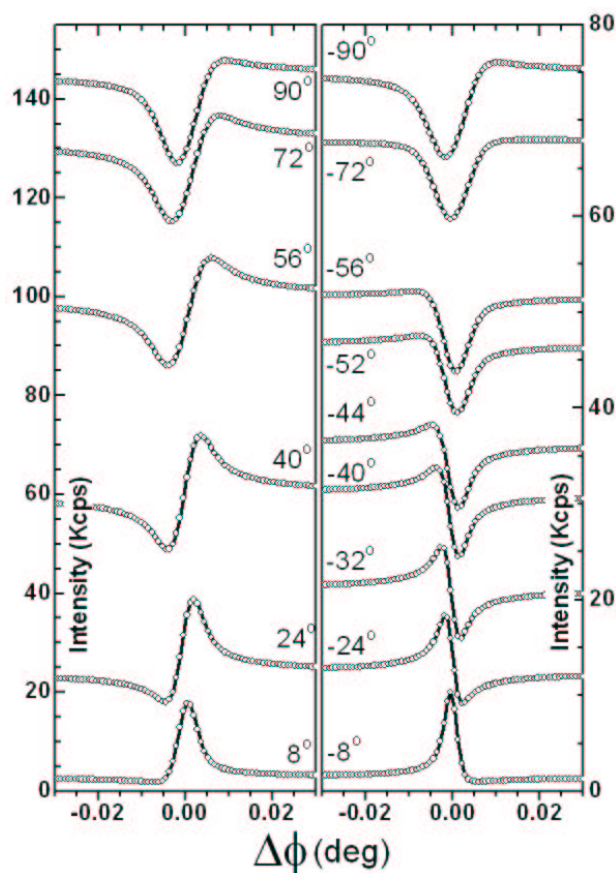
Figure 7
Three-beam X-ray diffraction interference profiles, ϕ-scans, generated by the *3rd*-order solution of the intensity equation, $\mathtt{I}_{A[3]}(\phi)$, for the same polarizations of the experimental scans in Fig. 5. The simulation parameters are: $2\theta_A = 2\theta_B = 89.997°$, $2\theta_C = 50.478°$, $[r_A\ r_B\ r_{\bar{A}}\ r_{\bar{C}}\ r_{\bar{B}}\ r_C] = [0.31\ 0.49\ 0.025\ 0.455\ 0.092\ 0.758]$ ($a_A = 0 \Rightarrow b = 0.466$), $w = 0.0016°$, $\xi_{\alpha\beta} = 0.6$ (for $\alpha \neq \beta$), $\Psi_T = 30.0°$, $\Delta\delta_A = \Delta\delta_B = \Delta\delta_C = 0.0°$, $\mathtt{I}_0 = 228$ Kcps and 441 Kcps for $\chi < 0°$ and $\chi > 0°$, respectively. The instrumental widths, w_G, are those obtained by fitting the experimental scans.

Recently, Stetsko *et al.* (2004) pointed out that for primary reflections with Bragg angle different of 45°, the diffracted wavefield of each individual channel in Eq. (15) would have different directions and behaviors as a function of the polarization direction. This is correct, as can be verified by the polarization factors provided in the Appendix A, Eqs. (22-26). However, this fact emphasizes the importance of developing theoretical approaches for the *3*-BD process that preserve the relative relevance of the channels, i.e. of the terms of the series expansion.

According to consistency of probabilities, the amplitude of a given channel does not depend only on the reflectivities of the involved reflections and polarization factors. They also depend on exiting probabilities as expressed, explicitly, by Eq. (19) in the Appendix A. The reflectivities determine the relative values of the diffraction probabilities, Eq. (18), and for $d_G+a_G > 0$, the sum of diffraction probabilities, $s_G = 1 - (d_G + a_G)$, are smaller than 1. Therefore, the amplitudes in Eq. (19) are, in modulus, smaller than they would be in an infinity non-absorbing crystal. The bottom line is that: diffraction geometry, absorption, and crystal shapes affect the relevance of the terms in a series expan-

sion of the primary wavefield. Accounting for such parameters would imply in lost of generality, i.e. of a general expression for describing all *3*-BD cases. This is the great advantage of the description presented here, based on consistency of probabilities.

Although we may not know yet how to estimate quantitatively the diffraction and exiting probabilities, any guess represents a real situation where the balance of energy among the diffracted beams is obeyed, as well as the relevance of each term of the series expansion. That is how was possible to reproduce (Fig. 6) an experimental dataset (Fig. 5) without providing any information about the sample. Even so, *Aufhellung* was taken into account, as well as the contributions of the *3rd*-order terms; see for instance, the asymmetric dip-like profile of the experimental scan in Fig. 7(a), whose asymmetry is a *3rd*-order feature owing to the A+$\bar{C}$+C channel.

Moreover, we have noticed that the set of diffraction probabilities responsible for the simulated scans, Fig. 6, provides the value of $R = \sqrt{r_B r_C / r_A} \approx 1.1$. According to Eq. (20), $R > 1$ leads to $|F_B| > |F_A|$ where the A and B reflections are the $\bar{2}26$ and $\bar{2}\bar{2}6$ reflections, respectively. Sphero-symmetric charge distributions placed at the atomic sites of the zinc-blend structure do not explain such inequality, even when anomalous dispersion corrections are considered.

The inaccuracies on the simulation parameter values are significant. They arrive mostly because the instrumental width is at least twice the intrinsic width, $w_G > 2w$. It increases the range of possible values capable to reproduce the same ϕ-scan. Otherwise, accurate R and Ψ_T values provide precious information on chemical bounding charges (Stahn *et al.*, 1999). A simple crystal structure model can explain $R \simeq 1.1$ and $\Psi_T = 30°$. In this model, 8 valence electrons (5 from Sb and 3 from Ga atoms) give rise to four bounding-charges, $2e^-$ each, placed at the fractional positions $x(1,1,1)$, $x(-1,-1,1)$, $x(-1,1,-1)$, and $x(1,-1,-1)$. With the unit cell origin at Sb and $x = 0.37/4$, the following structure factors and invariant phases are obtained after anomalous dispersion corrections: $|F_A| = |F_{\bar{A}}| = 40.8$, $|F_B| = |F_{\bar{B}}| = 47.2$, $|F_C| = 157.8$, $|F_{\bar{C}}| = 179.6$, $\Psi_T = 29.8°$, $\Delta\delta_A = 18.1°$, $\Delta\delta_B = 63.0°$, and $\Delta\delta_C = 13.8°$. The same s_G values used in the previous simulation, Fig. 6, provide $R = 1.047$ and a very close match to the set of diffraction probabilities, as well as to the simulated scans.
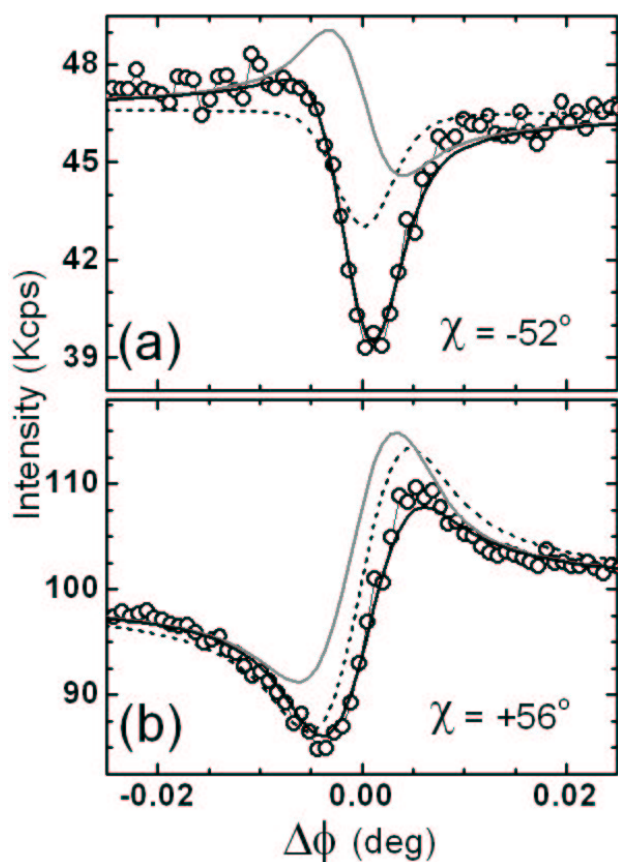
Figure 8
Experimental (open circles) three-beam X-ray diffraction profiles taken at polarizations where (a) $D_{BC} \approx D_{B\bar{B}A} \approx 0$ ($\chi = -52°$) and (b) their modulus are close to the maximum values ($\chi = 56°$). The simulated ϕ-scans generated by the *3rd*-order solution of the intensity equation, Eq. (16), stand for different situations: the same simulated scans in Fig. 6 with *Aufhellung* (black lines), without *Aufhellung*, i.e. $b = 0$ (gray lines), and without *Aufhellung* and $\Delta\delta_C = 80.0°$ (dashed lines).

5. Conclusions

It has been theoretically and experimentally demonstrated here that, when the three-beam X-ray diffraction phenomenon is described by approximated solutions in form of simple series expansions of the diffracted wavefields, mechanisms accounting for the balance of energy among the simultaneously diffracted beams are missing. The proposed theoretical approach succeeds in providing one of such mechanisms. Moreover, with this approach, it is possible to analyze experimental results and extract accurate information on the crystalline structure without the necessity of applying specific boundary conditions.

Appendix A.
Wavefield amplitudes

According to consistency of probabilities, the amplitude of the wavefield diffracted by each individual channel, or term of

the series expansion of the total wavefield, depend on diffraction probabilities, r_H, and polarization factors, $\nu_{channel}$. Up to the *3rd*-order solution of the primary wavefield, Eq. (15), the amplitude values (with $KD_0^2 = I_0$) are given by

$$
\begin{aligned}
\boldsymbol{D}_A &= \sqrt{r_A} D_0 \boldsymbol{\nu}_A \\
\boldsymbol{D}_{BC} &= \sqrt{r_B r_C} D_0 \boldsymbol{\nu}_{BC} \\
\boldsymbol{D}_{A\bar{A}A} &= \sqrt{r_A r_{\bar{A}} r_A} D_0 \boldsymbol{\nu}_{A\bar{A}A} \\
\boldsymbol{D}_{B\bar{B}A} &= \sqrt{r_B r_{\bar{B}} r_A} D_0 \boldsymbol{\nu}_{B\bar{B}A} \\
\boldsymbol{D}_{A\bar{C}C} &= \sqrt{r_A r_{\bar{C}} r_C} D_0 \boldsymbol{\nu}_{A\bar{C}C}.
\end{aligned}
\tag{17}
$$

In this appendix, the diffraction probabilities are related to the modulus square of the structure factors, $|F_H|$, and the polarization factors calculated from $2\theta_A$, $2\theta_B$, and $2\theta_C$, the angles between the diffracted beam directions.

A.1. Diffraction probabilities

The diffraction probabilites have been estimated by the following expressions assuming previous knowledge on the crystal structure, i.e. on the $|F_H|$ values:

$$
\begin{aligned}
r_A = s_0 |\tilde{F}_A|^2, \; r_B = s_0 |\tilde{F}_B|^2, \; r_{\bar{A}} = s_A |\tilde{F}_{\bar{A}}|^2, \\
r_{\bar{C}} = s_A |\tilde{F}_{\bar{C}}|^2, \; r_{\bar{B}} = s_B |\tilde{F}_{\bar{B}}|^2, \; \text{and } r_C = s_B |\tilde{F}_C|^2.
\end{aligned}
\tag{18}
$$

$s_G = 1 - (d_G + a_G)$, d_G and a_G are the exiting and absorption probabilities for X-ray photons in the beam G, and

$$
|\tilde{F}_{A,B}|^2 = |F_{A,B}|^2 / \left(|F_A|^2 + |F_B|^2 \right),
$$

$$
|\tilde{F}_{\bar{A},\bar{C}}|^2 = |F_{\bar{A},\bar{C}}|^2 / \left(|F_{\bar{A}}|^2 + |F_{\bar{C}}|^2 \right), \; \text{and}
$$

$$
|\tilde{F}_{\bar{B},C}|^2 = |F_{\bar{B},C}|^2 / \left(|F_{\bar{B}}|^2 + |F_C|^2 \right).
$$

In terms of the normalized structure factors and of s_G, the five amplitudes in Eq. (17) are written as

$$
\begin{aligned}
\boldsymbol{D}_A &= \sqrt{s_0} \, |\tilde{F}_A| D_0 \boldsymbol{\nu}_A \\
\boldsymbol{D}_{BC} &= \sqrt{s_0 \, s_B} \, |\tilde{F}_B||\tilde{F}_C| D_0 \boldsymbol{\nu}_{BC} \\
\boldsymbol{D}_{A\bar{A}A} &= s_0 \sqrt{s_A} \, |\tilde{F}_A||\tilde{F}_{\bar{A}}||\tilde{F}_A| D_0 \boldsymbol{\nu}_{A\bar{A}A} \\
\boldsymbol{D}_{B\bar{B}A} &= s_0 \sqrt{s_B} \, |\tilde{F}_B||\tilde{F}_{\bar{B}}||\tilde{F}_A| D_0 \boldsymbol{\nu}_{B\bar{B}A} \\
\boldsymbol{D}_{A\bar{C}C} &= \sqrt{s_0 \, s_A \, s_B} \, |\tilde{F}_A||\tilde{F}_{\bar{C}}||\tilde{F}_C| D_0 \boldsymbol{\nu}_{A\bar{C}C}.
\end{aligned}
\tag{19}
$$

In general, the interference profiles of the *3*-BDs are very much affected by two parameters: *i)* the amplitude ration (without polarization factors), R, between the 1*st* and 2*nd* terms of the series expansion, i.e. between the wavefields from channels A and B+C, which depends on s_B according to

$$
R = \sqrt{\frac{r_B r_C}{r_A}} = \sqrt{s_B} \frac{|\tilde{F}_B||\tilde{F}_C|}{|\tilde{F}_A|};
\tag{20}
$$

and *ii)* the fraction of *Aufhellung*, b, given by

$$
b = s_A \frac{|\tilde{F}_{\bar{C}}|^2}{1 - a_A - s_A |\tilde{F}_{\bar{A}}|^2}.
\tag{21}
$$

Note that s_B and s_A account for absorption and exinting probabilities, and therefore, the effects of such probabities in the interference profiles.

A.2. Polarization factors

For a linearly polarized X-ray incident beam, whose polarization direction is given by the unit vector $\hat{v}_0$, the polarization factors are calculated as (Thorkildsen & Larsen, 2002; Stetsko et al., 2004)

$$v_A = \hat{k}_A \times (\hat{v}_0 \times \hat{k}_A) \tag{22}$$
$$v_B = \hat{k}_B \times (\hat{v}_0 \times \hat{k}_B)$$
$$v_{BC} = \hat{k}_A \times (v_B \times \hat{k}_A) \tag{23}$$
$$v_{A\bar{A}} = \hat{k}_0 \times (v_A \times \hat{k}_0)$$
$$v_{A\bar{A}A} = \hat{k}_A \times (v_{A\bar{A}} \times \hat{k}_A) \tag{24}$$
$$v_{B\bar{B}} = \hat{k}_0 \times (v_B \times \hat{k}_0)$$
$$v_{B\bar{B}A} = \hat{k}_A \times (v_{B\bar{B}} \times \hat{k}_A) \tag{25}$$
$$v_{A\bar{C}} = \hat{k}_B \times (v_A \times \hat{k}_B)$$
$$v_{A\bar{C}C} = \hat{k}_A \times (v_{A\bar{C}} \times \hat{k}_A) \tag{26}$$

where $\hat{k}_G$ is an unit vector along the propagation direction of the beam G. For sake of simplicity, these directions are calculated here from the $2\theta_A$, $2\theta_B$, and $2\theta_C$ values, according to: $\hat{k}_0 = [0, 0, 1]$, $\hat{k}_A = [\sin 2\theta_A, 0, \cos 2\theta_A]$, and $\hat{k}_B = [x, y, \cos 2\theta_B]$ where

$$x = \frac{\cos 2\theta_B - \cos 2\theta_A \cos 2\theta_B}{\sin 2\theta_A}$$

and

$$y = \pm\sqrt{\sin^2 2\theta_B - x^2}.$$

In this reference system, the polarization direction of the incident radiation is written as $\hat{v}_0 = [-\cos\chi, \sin\chi, 0]$. The minus signal is owing to the rotation sense of the diffractometer's χ-axis.

References

Batterman, B. W. & Cole, H. (1964). *Rev. Mod. Phys.* **36**, 681-717.
Chang, S.-L. (1984). *Multiple Diffraction of X-Rays in Crystals*. New York: Springer Verlag.
Chang, S.-L. & Tang, M. T. (1988). *Acta Cryst.* A**44**, 1065-1070.
Chang, S.-L. (1998). *Acta Cryst.* A**54**, 886-894.
Colella, R. (1995). *Commun. Condens. Matter Phys.* **17**, 175-215.
Darwin, C. G. (1914). *Phil. Mag.* **27**, 315-xxx and 675-xxx.
Ewald, P. P. (1917). *Ann. Physik* **54**, 519-597.
Høier, R. & Marthinsen, K. (1983). *Acta Cryst.* A**39**, 854-861.
Hümmer, K. & Billy, H. (1986). *Acta Cryst.* A**42**, 127-133.
Juretschke, H. J. (1982). *Phys. Rev. Lett.* **48**, 1487-1490.
Kato, N. (1976). *Acta Cryst.* A**32**, 453-464.
Loudon, R. (2000). *The Quantum Theory of Light*. Oxford University Press.
Morelhão, S. L. & Kycia, S. (2002). *Phys. Rev. Lett.* **89**, 015501.
Morelhão, S. L. (2003). *J. Synchrotron Rad.* **10**, 236-241.
Okitsu, K. (2003). *Acta Cryst.* A**59**, 235-346.
Renninger, M. (1937). *Z. Kristallogr.* **97**, 107-121.
Shen, Q. (1986). *Acta Cryst.* A**42**, 525-533.
Shen, Q. & Finkelstein, K. D. (1990). *Phys. Rev. Lett.* **65**, 3337-3340.
Shen, Q., Kycia, S. & Dobrianov, I. (2000). *Acta Cryst.* A**56**, 268-278.
Shen, Q. & Huang, X. R. (2001). *Phys. Rev. B* **63**, 174102-174112.
Stahn, J., Pucher, A., Pietsch, U., Zellner, J. & Weckert, E. (1999). *Acta Cryst.* A**55**, 1034-1037.
Stetsko, Yu. P., Lin, G. Y., Huang, Y.S., Chao, C. H. & Chang, S. L. (2001a). *Phys. Rev. Lett.* **86**, 2026-2029.
Stetsko, Yu. P., Juretschke, H. J., Huang, Y.S., Lee, Y. R., Lin, T. C. & Chang, S. L. (2001b). *Acta Cryst.* A**57**, 359-364.
Stetsko, Yu. P., Lee, Y. R., Tang, M. T. & Chang, S. L. (2004). *Acta Cryst.* A**60**, 64-74.
Thorkildsen, G., Larsen, H. B. & Weckert, E. (2001). *Acta Cryst.* A**57**, 389-397.
Thorkildsen, G. & Larsen, H. B. (2002). *Acta Cryst.* A**58**, 252-259.
Thorkildsen, G., Larsen, H. B., Weckert, E. & Semmingsen, D. (2003). *Acta Cryst.* A**36**, 1324-1333.
Wagner, E. (1923). *Phyz. Z.* **21**, 94-98.
Weckert, E. & Hümmer, K. (1997). *Acta Cryst.* A**53**, 108-143.
Zachariasen, W. H. (1945). *Theory of X-Rays Diffraction in Crystals*. John Wiley & Sons, Inc., New York.